Interdiffusion, Solubility Limit, and Role of Entropy in FCC Al-Co-Cr-Fe-Ni Alloys

ABHISHEK MEHTA and YONGHO SOHN

High entropy and sluggish diffusion "core" effects were investigated in an FCC Al-Co-Cr-Fe-Ni alloy by examining the nonequiatomic compositions generated by the concentration profiles within the solid-to-solid diffusion couple, $Al_{48}Ni_{52}$ *vs* $Co_{25}Cr_{25}Fe_{25}Ni_{25}$, annealed at 900 °C, 1000 °C, 1100 °C, and 1200 °C. The average effective interdiffusion coefficients of individual components and the maximum solubility limit of Al in nonequiatomic Al-Co-Cr-Fe-Ni alloys were determined as a function of temperature. The magnitudes of the average effective interdiffusion coefficients in Al-Co-Cr-Fe-Ni alloys were compared to the interdiffusion coefficients in relevant ternary and quaternary alloys. The solubility limit of Al in nonequiatomic $Al_pCo_qCr_rFe_sNi_t$ alloys was compared to that of Al in equiatomic $Al_xCoCrFeNi$ determined from the equilibrium pseudo-binary phase diagram. A reduction in the magnitude of interdiffusion coefficients was not observed for individual components in Al-Co-Cr-Fe-Ni alloys. The maximum solubility of Al in nonequiatomic $Al_pCo_qCr_rFe_sNi_t$ alloys was observed to be higher than that in equiatomic $Al_xCoCrFeNi$ alloys at a temperature of 1100 °C or above. Correspondingly, the free energy of mixing for nonequiatomic $Al_pCo_qCr_rFe_sNi_t$ alloys was determined to be lower than that of equiatomic $Al_xCoCrFeNi$ alloys at a temperature of 1100 °C or above. At a temperature of 1100 °C or above, the role of enthalpy of mixing was estimated to be significant in achieving higher thermodynamic stability of the nonequiatomic $Al_pCo_qCr_rFe_sNi_t$ alloy than in the equiatomic $Al_xCoCrFeNi$ alloy for the compositions corresponding to the highest solubility limit for Al. The compositions of nonequiatomic $Al_pCo_qCr_rFe_sNi_t$ alloys were observed to follow the existing empirical rules for the formation of single phase in high entropy alloys (HEAs).

https://doi.org/10.1007/s11661-020-05742-z

I. INTRODUCTION

HIGH entropy alloys (HEAs) were proposed to exhibit four "core" effects: high entropy, sluggish diffusion, lattice distortion, and cocktail effect.[1] Except for the cocktail effect, all other core effects may not be significant as were first proposed.[2] The mechanism of stabilization of single phase, *i.e.*, the high entropy effect, initially hypothesized that a large number of constituent elements in an equal amount would increase the entropy of mixing, which would lower the overall Gibb's free energy of mixing, particularly at high temperatures. This is true as the entropic contribution is typically higher than the enthalpy contribution toward the overall thermodynamic stability of HEAs, *i.e.*, $|-T\Delta S| > |\Delta H|$, at high temperature. Therefore, high entropy phases, *e.g.*, random/disordered solid solution phases, would be stabilized in comparison to low entropy phases, *e.g.*, intermetallic phases. The theory on entropic stabilization of phases due to high configurational entropy, however, falls short in regard to explaining the multiple phases observed in various experimental, near-equiatomic alloys, *e.g.*, AlCoCrFeNi,[3] AlCoCrFeNiMn,[4] and CoCrFeNiMo.[5] Intuitively, a simple replacement of an element in an HEA by another element would not ensure the formation of single-phase solid solution, *e.g.*, replacing Mn with either Al or Mo in single-phase, equiatomic CoCrFeNiMn alloy. Therefore, entropy of mixing alone may not always result in lowering of the Gibbs free energy.[6] Otto *et al.*[7] also suggested that an increase in configurational entropy may not stabilize the single phase in all alloys, since this effect may not be sufficient to overcome the driving forces that favor the formation of secondary phases.

The diffusion in HEAs was hypothesized to be sluggish.[8] Various studies[8–15] have been carried out to determine the tracer diffusion coefficients. There has been no common consensus on the sluggish diffusion hypothesis: Some studies reported that diffusion is

ABHISHEK MEHTA and YONGHO SOHN are with the Department of Materials Science and Engineering, Advanced Materials Processing and Analysis Center, University of Central Florida, Orlando, FL 32816. Contact e-mail: Yongho.Sohn@ucf.edu
Manuscript submitted October 10, 2019.
Article published online April 19, 2020

indeed sluggish in HEAs, while others did not. In potential engineering applications where diffusion may occur under the concentration gradients, interdiffusion coefficients that combine the influence of both the thermodynamics and kinetics may be more relevant. Limited studies[12,16,17] have examined the interdiffusion in HEAs; however, no relevant comparison was made to elucidate the possible "sluggish diffusion" in HEAs.

In this study, two core effects, *i.e.*, high entropy and sluggish diffusion, were examined in Al-Co-Cr-Fe-Ni alloys using solid-to-solid diffusion couple investigation as it can generate many local equilibrium compositions. The β-$Al_{48}Ni_{52}$ *vs* $Co_{25}Cr_{25}Fe_{25}Ni_{25}$ diffusion couple was annealed at 900 °C, 1000 °C, 1100 °C, and 1200 °C. These diffusion couples generated continuous compositions of nonequiatomic $Al_pCo_qCr_rFe_sNi_t$ alloys. The average effective interdiffusion coefficients and solubility limit of Al in $Al_pCo_qCr_rFe_sNi_t$ alloy were determined as a function of temperature. Interdiffusion coefficients were compared with interdiffusion coefficients of various elements in relevant ternary and quaternary alloys. The solubility limit of Al in nonequiatomic $Al_pCo_qCr_rFe_sNi_t$ was also compared with the solubility limit of Al in high entropy $Al_xCoCrFeNi$ alloy. Results were analyzed with regard to the contributions from enthalpy (ΔH) and entropy ($-T\Delta S$) to the thermodynamic stability (ΔG) of equiatomic and nonequiatomic Al-Co-Cr-Fe-Ni alloys.

II. EXPERIMENTAL METHOD

The single-phase solid solutions of β-$Al_{48}Ni_{52}$ (B2) and FCC $Co_{25}Cr_{25}Fe_{25}Ni_{25}$ alloys were prepared using pure Al, Co, Cr, Fe, and Ni procured from Alfa-Aesar with minimum 99.9 pct purity (*i.e.*, Al: 99.99 pct, Co: 99.9+ pct, Cr: 99.99 pct, Fe: 99.98 pct, and Ni: 99.95 pct). Alloys were prepared by arc melting, with a water-cooled Cu crucible in an argon atmosphere. Alloy ingots were cast and remelted 5 times, by flipping the ingot after each melting to promote the initial compositional homogeneity. All alloy ingots were further subjected to homogenization heat treatment in a quartz-encapsulated argon atmosphere at 1100 °C for 48 hours and subsequently water quenched. Phase constituents (*e.g.*, single-phase formation) and microstructural homogeneity were examined by a Malvern Panalytical Empyrean X-ray diffraction system with a 1.8 kW Cu X-ray tube operating at 45 keV voltage and 40 mA current. A Cu K_α radiation source with wavelength of 1.54 Å was used. For each alloy sample, X-ray diffraction (XRD) was performed with a step size of 0.033 deg and a dwell time of 60 seconds. Compositional examination was performed using a Zeiss Ultra-55 field emission-scanning electron microscope (FE-SEM) equipped with Thermo-Scientific X-ray energy dispersive spectroscopy (XEDS).

For solid-to-solid diffusion couple experiments, single-phase β-$Al_{48}Ni_{52}$ (B2) and FCC $Co_{25}Cr_{25}Fe_{25}Ni_{25}$ alloys were sectioned into discs (10 mm in diameter and 3 mm in height) and metallographically polished down to 1-μm surface finish. Diffusion couples were assembled by placing the polished surfaces of β-$Al_{48}Ni_{52}$ and $Co_{25}Cr_{25}Fe_{25}Ni_{25}$ alloys in intimate contact. The alloys in the diffusion couple were held tightly by two stainless steel jigs and clamped together with screws. Thin alumina spacers were placed between the alloy and stainless steel jig to avoid any interdiffusion between the alloys and jigs. The assembled diffusion couple along with a tantalum foil (*i.e.*, oxygen getter) was placed in a quartz tube, evacuated to a pressure of 8×10^{-6} torr or better, and flushed alternately with high-purity Ar and H_2 gas. The evacuation and flushing procedure was repeated several times before the quartz tube was sealed, creating a closed, high-purity Ar atmosphere for the diffusion couples. More details of diffusion couple fabrication can be found elsewhere.[18–20] The diffusion couple was isothermally annealed at 900 °C, 1000 °C, 1100 °C, and 1200 °C for 240, 120, 48, and 24 hours, respectively. After annealing, all diffusion couples were water quenched to preserve the high-temperature microstructure. Then, each diffusion couple was mounted in cold resin epoxy and cross sectioned normal to the metal-metal interface. Finally, all diffusion couples were metallographically polished down to 1-μm surface finish. Microstructural examination and concentration profile measurement were performed using a Zeiss Ultra-55 FE-SEM, equipped with Thermo-Scientific XEDS. A minimum of three XEDS linescans were carried out to determine the concentration profiles in each diffusion couple to ensure statistical confidence. The maximum solubility limit of Al in nonequiatomic FCC $Al_pCo_qCr_rFe_sNi_t$ alloy was performed 5 μm away from the interface boundary on the FCC side of the $Al_{48}Ni_{52}$ *vs* $Co_{25}Cr_{25}Fe_{25}Ni_{25}$ diffusion couple, to avoid the effect of interaction volume from the $Al_{48}Ni_{52}$ BCC side. To ensure the statistical consistency, multiple measurements were performed to measure the maximum solubility limit of the Al in nonequiatomic FCC $Al_pCo_qCr_rFe_sNi_t$ alloy at the interface boundary.

III. ANALYTICAL FRAMEWORK

A. *Interdiffusion Coefficients*

Onsager's formalism,[21] based on irreversible thermodynamics, is generally employed to understand the interdiffusion flux in multicomponent alloys. A general expression of interdiffusion flux, $\tilde{J}_i$ for an individual component in an n-component system is given by

$$\tilde{J}_i = -\sum_{j=1}^{n-1} \tilde{D}_{ij}^{n} \frac{\partial C_j}{\partial x} (i = 1, 2, \ldots, n-1) \qquad [1]$$

$\tilde{D}_{ij}^{n}$ represents the $(n-1)^2$ interdiffusion coefficients and $\partial C_j/\partial x$ represents the concentration gradients. When the composition-dependent variation of molar volume is negligible, interdiffusion flux at any plane x can be determined from the concentration profiles without the knowledge of interdiffusion coefficients using the following relationship[22]:

$$\tilde{J}_i = \frac{1}{2t} \int_{C_i(\pm\infty)}^{C_i(x)} (x - x_0)\mathrm{d}C_i (i = 1, 2 \ldots, n-1) \quad [2]$$

An extension of the Boltzmann–Matano analysis in the multicomponent system then can be employed to measure the interdiffusion coefficients,[23] as expressed by

$$\int_{C_i(\pm\infty)}^{C_i(x)} (x - x_0)\mathrm{d}C_i = -2t \sum_{j=1}^{n-1} \tilde{D}_{ij}^{n} \frac{\partial C_j}{\partial x} (i = 1, 2, \ldots, n-1) \quad [3]$$

However, measurement of interdiffusion coefficients using the preceding Boltzmann–Matano method is challenging for quaternary or higher component systems. For instance, in a quinary system, 4 independent compositional gradients are correlated to 4 independent interdiffusion fluxes by 16 interdiffusion coefficients at a fixed composition. This requires four different diffusion couples, but simply conducting these diffusion couple experiments does not ensure the successful determination of interdiffusion coefficients because the diffusion paths of four diffusion couples must intersect at a single composition in the five-dimensional compositional space of a Gibbs pentahedron.

A simplified representation of the interdiffusion coefficient was developed by Dayananda and Sohn[24] to determine the average effective interdiffusion coefficients for the multicomponent system with a single diffusion couple experiment. The average effective interdiffusion coefficient can be determined for any component over a desired composition range using the relation

$$\begin{aligned} \int_{x_1}^{x_2} \tilde{J}_i \, \mathrm{d}x &= -\overline{\tilde{D}}_i^{\mathrm{eff}} (C_i(x_1) - C_i(x_2)) \\ &= -\frac{1}{2t} \int_{C_i(x_1)}^{C_i(x_2)} (x - x_o)^2 \mathrm{d}C_i (i = 1, 2 \ldots, n) \end{aligned} \quad [4]$$

where $\overline{\tilde{D}}_i^{\mathrm{eff}}$ represents the average effective interdiffusion coefficient of component i for the composition range from $C_i(x_1)$ to $C_i(x_2)$. The average effective interdiffusion coefficient represents one magnitude for a single component, but it does not give any information about the main- and cross-interdiffusion coefficients.

Experimental concentration profiles measured from XEDS in this study were curve fitted using Origin Pro 8.5 software, with a nonlinear curve fitting function given by References 20, 25, and 26:

$$c(x) = \frac{p_1 + p_3 x + p_5 x^2 + p_7 x^3}{1 + p_2 x + p_4 x^2 + p_6 x^3} \quad [5]$$

B. *Potential Energy Fluctuations and Correlated Configurational Entropy*

Based on statistical thermodynamics, He *et al.*[27,28] derived a formula for normalized potential energy fluctuations (PEFs); *i.e.*, $p = \Delta E / k_{\mathrm{B}} T$, where ΔE represents the difference between maximum and minimum energy of the lattice site and $k_{\mathrm{B}} T$ represents the thermal energy fluctuations in HEAs. Atomic size mismatch and chemical bond mismatch are the two significant contributions to PEFs pertaining to HEAs. PEFs due to atomic size mismatch (p_e) and chemical bond mismatch (p_c) can be expressed as

$$p_e = 4.12\delta \sqrt{\frac{\bar{K}\bar{V}}{k_{\mathrm{B}} T}} \quad (i = 1, 2 \ldots, n) \quad [6]$$

and

$$p_c = 2\sqrt{\frac{\sqrt{\sum_j, \sum_{i \neq j} X_i X_j (\Delta H_{ij}^{\mathrm{mix}} - \bar{H})^2}}{k_{\mathrm{B}} T}} \quad (i = 1, 2 \ldots, n-1; \quad j = i+1) \quad [7]$$

where δ represents the atomic size mismatch parameter, as described in Section III–C, $\bar{K}$ is the composition-weighted average bulk modulus, $\bar{V}$ is the composition-weighted average atomic volume, and $\Delta H_{ij}^{\mathrm{mix}}$ is the binary enthalpy of mixing, which can be estimated using the Miedema's macroscopic model for liquid binary alloy.[29,30] Therefore, PEFs can be defined by the sum of Eqs. [6] and [7] as

$$p = 4.12\delta \sqrt{\frac{\bar{K}\bar{V}}{k_{\mathrm{B}} T}} + 2\sqrt{\frac{\sqrt{\sum_i \sum_{j, i \neq j} X_i X_j (\Delta H_{ij}^{\mathrm{mix}} - \bar{H})^2}}{k_{\mathrm{B}} T}} \quad [8]$$

Boltzmann entropy is applicable to an isolated system under thermodynamic equilibrium, while the Gibbs entropy can be applicable to metastable states in addition to equilibrium states.[31] He *et al.*[27] demonstrated that the ideal entropy of mixing (ΔS_{mix}) overestimates the entropy of mixing due to a correlation effect between constituent elements. This correlation depends on the difference in bond strengths and atomic size mismatch of the constituent elements in the alloy. A significant correlation effect in an alloy system gives rise to a larger variation in lattice potential energy (LPE) and excess entropy (S_E). Using the statistical thermodynamics, He *et al.* developed a phenomenology to describe excess configurational entropy by considering the general effects of PEFs (*i.e.*, Eq. [8]), given by

$$S_E = k_{\mathrm{B}} \times \left[1 + \frac{p}{2} - \ln(p) + \ln(1 - e^{-p}) - \frac{p}{2} \times \frac{1 + e^{-p}}{1 - e^{-p}}\right] \quad [9]$$

The correlated configurational entropy of mixing (ΔS_{corr}) can be expressed by the sum of ideal and excess entropy terms. Therefore, the final expression for the entropy under correlated mixing can be expressed as

$$\Delta S_{corr} = -k_B \sum_{i=1}^{n} (X_i \ln X_i) + k_B \times \left[1 + \frac{p}{2} - \ln(p) + \ln(1 - e^{-p}) - \frac{p}{2} \times \frac{1 + e^{-p}}{1 - e^{-p}}\right] \quad [10]$$

C. *Solid-Solution Phase Formation Rules Pertaining to HEAs*

Hume–Rothery rules provide a guideline for binary alloys that describes the conditions under which an alloying element can dissolve in solvent as a substitutional solute. Elements with similar atomic size, crystal structure, valency, and electronegativity have more solubility in each other. Various researchers have mathematically extended the Hume–Rothery rules to multicomponent alloys, especially when solute and solvent cannot be distinguished, *e.g.*, HEAs or bulk metallic glasses. The δ parameter is adopted as a measure of mismatch in atomic size for multicomponent alloys, expressed by[32]

$$\delta = \sqrt{\sum_{i=1}^{n} X_i \left(1 - \frac{r_i}{\sum X_i r_i}\right)^2} \quad [11]$$

where r_i is the atomic radius of an individual component i. ΔH_{mix} is a parameter used to predict the chemical compatibility among the constituent elements, which is given by[33]

$$\Delta H_{mix} = \sum_{i=1}^{n-1} \sum_{j=2, i>j}^{n} (4 \times \Delta H_{ij}^{mix}) X_i X_j \quad [12]$$

where $4 \times \Delta H_{ij}^{mix}$ is the regular solution interaction parameter between components i and j. The ΔH_{mix} is an important predictor for the formation of disordered single-phase solid solution. Alloys will exhibit the higher disordered solid solution formation tendency if the value of ΔH_{mix} approaches zero. Recently, Yang and Zhang[34] describes the Ω parameter, which accounts for the relative effects for enthalpy of mixing and entropy of mixing, given by[33]

$$\Omega = \frac{T\Delta S_{mix}}{|\Delta H_{mix}|} \quad [13]$$

where ΔS_{mix} ($-R \sum X_i \ln X_i$) is the Boltzmann entropy of mixing. In as-cast alloys, T is adopted as the melting temperature of the alloy, measured using the simple rule of mixtures. However, in the present study, alloy compositions were fabricated *via* diffusion under isothermal condition. Therefore, T is defined as the temperature of diffusion anneal.

The difference in electronegativity ($\Delta\chi$) between constituent elements in HEAs is measured as a root-mean-square of the composition-weighted average for the deviation in electronegativity from the mean value in HEAs as[32]

$$\Delta\chi = \sqrt{\sum_{i=1}^{n} X_i \left(\chi_i - \sum X_i \chi_i\right)^2} (i = 1, 2, \ldots, n) \quad [14]$$

where χ_i is the Pauling electronegativity of individual components. Electron concentration in HEAs can be estimated as either valence electron concentration (VEC) or electron per atom (e/a ratio). VEC is typically considered more relevant than the e/a ratio since VEC represents a more realistic electronic band structure when first-principles band calculations are used for determination of the Fermi level.[35] VEC can be determined in HEAs as a composition-weighted average VEC value of the constituent elements[36]:

$$\text{VEC} = \sum X_i (\text{VEC})_i (i = 1, 2, \ldots, n) \quad [15]$$

IV. INTERDIFFUSION COEFFICIENTS

Figure 1 presents the XRD patterns, and Table I outlines the average compositions of homogenized B2-$Al_{48}Ni_{52}$ and FCC-$Co_{25}Cr_{25}Fe_{25}Ni_{25}$ alloys. Figure 2 presents the concentration profiles superimposed on backscatter electron micrographs from the $Al_{48}Ni_{52}$ *vs* $Co_{25}Cr_{25}Fe_{25}Ni_{25}$ diffusion couples isothermally annealed at (a) 900 °C for 240 hours, (b) 1000 °C for 120 hours, (c) 1100 °C for 48 hours, and (d) 1200 °C for 24 hours. The concentration profiles of Ni exhibit

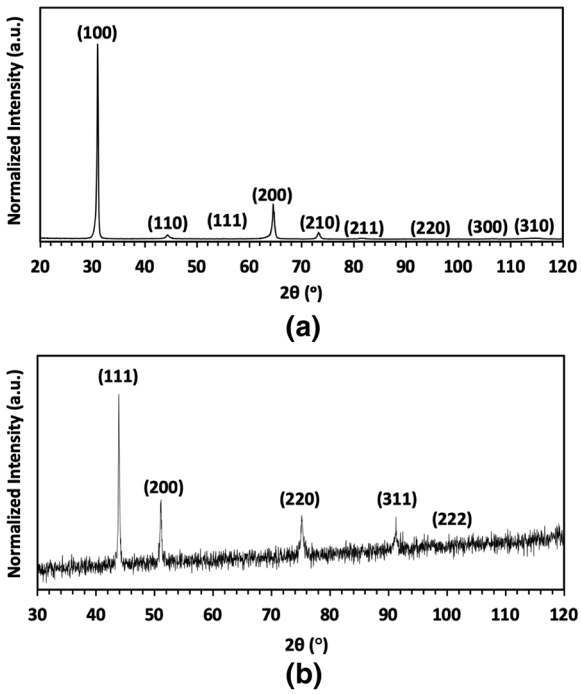

Fig. 1—XRD patterns from the homogenized (*a*) $Al_{48}Ni_{52}$ and (*b*) $Co_{25}Cr_{25}Fe_{25}Ni_{25}$ alloys examined in this study.

Table I. Compositions of the Homogenized Alloys Employed in This Study with Corresponding Lattice Parameter and Crystal Structure Determined from XRD

Alloys	Al (At. Pct)	Co (At. Pct)	C (At. Pct)	Fe (At. Pct)	Ni (At. Pct)	Lattice Parameters (Å)	Crystal Structure
$Al_{48}Ni_{52}$	48.10 (0.29)	—	—	—	51.90 (0.34)	2.89 (0.00)	BCC (B2)
$Co_{25}Cr_{25}Fe_{25}Ni_{25}$	—	24.73 (0.2)	25.77 (0.36)	25.28 (0.23)	24.22 (0.19)	3.58 (0.00)	FCC ($L1_2$)

Composition values in parenthesis correspond to standard deviation from 10 random location measurements.

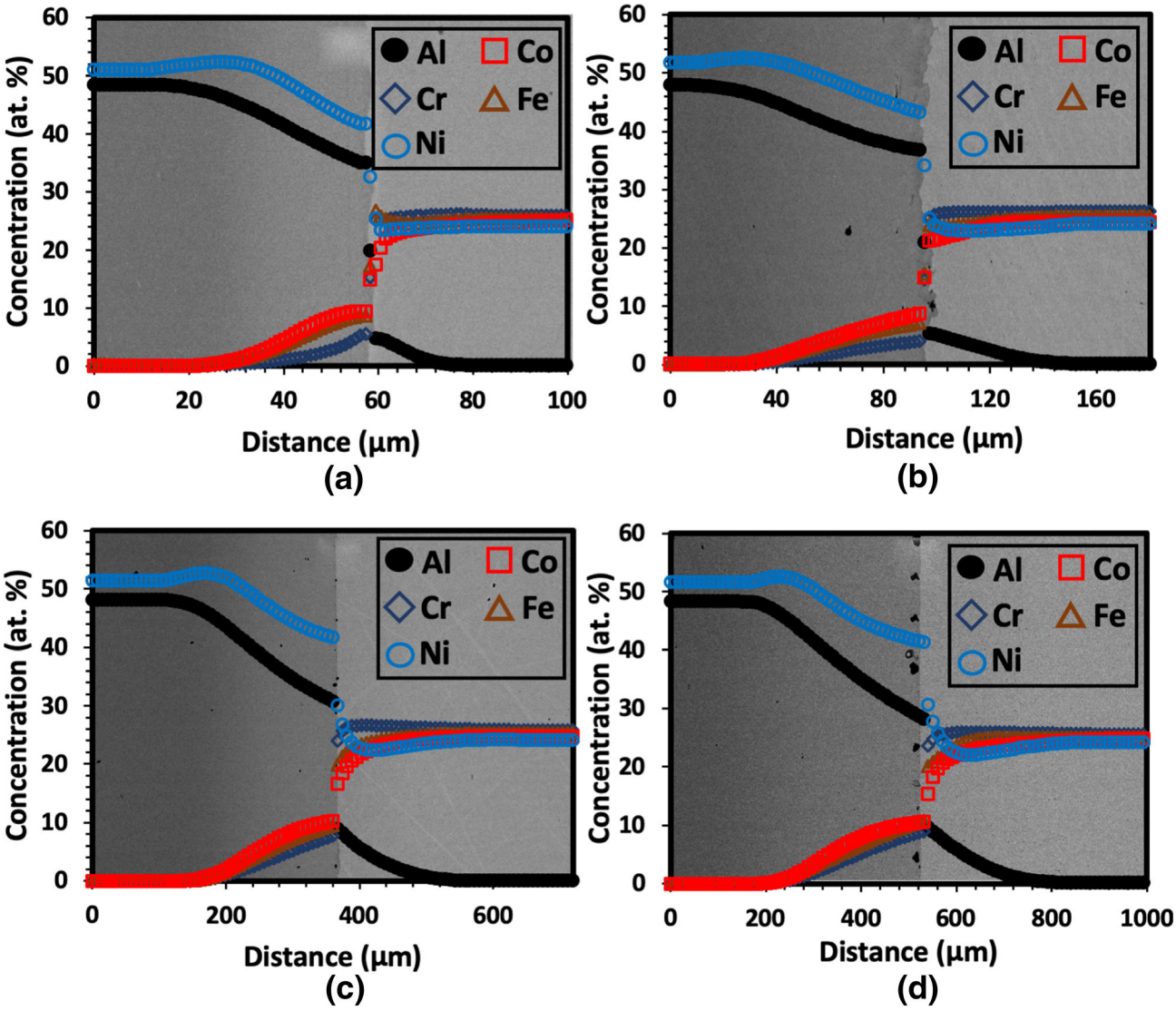

Fig. 2—Concentration profiles superimposed on backscatter electron micrographs from $Al_{48}Ni_{52}$ *vs* $Co_{25}Cr_{25}Fe_{25}Ni_{25}$ diffusion couples isothermally annealed at (*a*) 900 °C for 240 h, (*b*) 1000 °C for 120 h, (*c*) 1100 °C for 48 h, and (*d*) 1200 °C for 24 h.

the phenomena of uphill diffusion, exhibited by the relative maxima, at all temperatures on the β-$Al_{48}Ni_{52}$ side due to the increase in chemical potential of Ni. Kirkendall voids were observed in the microstructure on the β-$Al_{48}Ni_{52}$ side, close to the AlNi/CoCrFeNi interphase boundary. The presence of Kirkendall porosity on the β-$Al_{48}Ni_{52}$ side demonstrates that either the Al or Ni intrinsically diffuses faster than Co, Cr, or Fe, which leaves excess vacancies on the β-$Al_{48}Ni_{52}$ side. Kirkendall voids form due to coalescence of excess vacancies.

Table II reports the average effective interdiffusion coefficients ($\overline{\tilde{D}}_i^{\text{eff}}$), activation energy, and pre-exponential factors for Al, Co, Cr, Fe, and Ni, determined on the β-$Al_{48}Ni_{52}$ side and $Co_{25}Cr_{25}Fe_{25}Ni_{25}$ alloy side. It should be noted that some values of interdiffusion coefficients for Cr and Ni are negative, which are related

to the existence of relative maxima and minima, respectively, in the Cr and Ni concentration profiles of Cr on the FCC side of the diffusion couple. This is due to the fact that the cross-interdiffusion (off-diagonal) coefficients may be larger in magnitude than the main-interdiffusion (diagonal) coefficients; *i.e.*, $\left|\tilde{D}_{ij}^{n}\right| > \left|\tilde{D}_{ii}^{n}\right|$.

Table III compares the average effective interdiffusion coefficients of Fe, Cr, and Ni in Fe-Cr-Ni alloy at 1100 °C[37] with the average effective interdiffusion coefficients of Fe, Cr, and Ni in Al-Co-Cr-Fe-Ni alloy. The comparison suggests that interdiffusion may be slower in the ternary Fe-Cr-Ni system than in the quinary Al-Co-Cr-Fe-Ni system. Furthermore, Table IV compares the average effective interdiffusion coefficients of Co, Cr, Fe, and Ni at 1000 °C in the quaternary Co-Cr-Fe-Ni,[16] quinary Co-Cr-Fe-Ni-Mn,[17] and quinary Al-Co-Cr-Fe-Ni systems. The interdiffusion diffusion coefficient of Cr is larger in the quinary Co-Cr-Fe-Ni-Mn system than in the quaternary Co-Cr-Fe-Ni and quinary Al-Co-Cr-Fe-Ni systems. The interdiffusion diffusion coefficient of Fe is larger in the quinary Al-Co-Cr-Fe-Ni system than in the quaternary

Table II. Average Effective Interdiffusion Coefficients ($\overline{\tilde{D}}_i^{\text{eff}}$), Activation Energy, and Pre-Exponential Factors for Al, Co, Cr, Fe, and Ni Determined from $Al_{48}Ni_{52}$ (B2) *vs* $Co_{25}Cr_{25}Fe_{25}Ni_{25}$ (FCC) Diffusion Couples

Component *i*	Temperature (°C)	$\overline{\tilde{D}}_i^{\text{eff}}$ (m^2/s) on the Side of B2-$Al_{48}Ni_{52}$	$\overline{\tilde{D}}_i^{\text{eff}}$ (m^2/s) on the Side of FCC-$Co_{25}Cr_{25}Fe_{25}Ni_{25}$
Al	900	$1.9\ (0.1) \times 10^{-16}$	$7.3\ (1.0) \times 10^{-17}$
	1000	$1.9\ (0.1) \times 10^{-15}$	$9.3\ (1.7) \times 10^{-16}$
	1100	$4.0\ (< 0.1) \times 10^{-14}$	$2.1\ (0.1) \times 10^{-14}$
	1200	$1.8\ (< 0.1) \times 10^{-13}$	$1.0\ (< 0.1) \times 10^{-13}$
	Q (kJ/mol) and D_0 (m^2/s)	339.71 and 0.23	357.42 and 0.57
Cr	900	$7.8\ (1.7) \times 10^{-17}$	$4.4\ (3.0) \times 10^{-17}$
	1000	$1.1\ (0.2) \times 10^{-15}$	$4.0\ (1.2) \times 10^{-16}$
	1100	$2.5\ (0.1) \times 10^{-14}$	$-2.7\ (1.1) \times 10^{-14}$
	1200	$1.2\ (0.1) \times 10^{-13}$	$-5.2\ (1.6) \times 10^{-14}$
	Q (kJ/mol) and D_0 (m^2/s)	363.49 and 1.15	—
Fe	900	$1.2\ (0.2) \times 10^{-16}$	$3.0\ (1.7) \times 10^{-16}$
	1000	$1.3\ (0.1) \times 10^{-15}$	$1.4\ (1.4) \times 10^{-15}$
	1100	$3.2\ (0.1) \times 10^{-14}$	$1.1\ (0.7) \times 10^{-14}$
	1200	$1.5\ (0.0) \times 10^{-13}$	$3.5\ (0.6) \times 10^{-14}$
	Q (kJ/mol) and D_0 (m^2/s)	352.10 and 0.52	233.71 and < 0.01
Co	900	$1.5\ (0.1) \times 10^{-16}$	$9.9\ (2.8) \times 10^{-17}$
	1000	$1.3\ (0.1) \times 10^{-15}$	$9.1\ (6.0) \times 10^{-16}$
	1100	$3.3\ (0.0) \times 10^{-14}$	$1.5\ (0.2) \times 10^{-14}$
	1200	$1.6\ (0.1) \times 10^{-13}$	$6.9\ (1.0) \times 10^{-14}$
	Q (kJ/mol) and D_0 (m^2/s)	346.61 and 0.35	322.67 and 0.02
Ni	900	$-2.0\ (0.8) \times 10^{-17}$	$3.0\ (2.2) \times 10^{-16}$
	1000	$5.0\ (2.0) \times 10^{-16}$	$-2.2\ (0.1) \times 10^{-15}$
	1100	$8.9\ (1.3) \times 10^{-15}$	$-1.2\ (0.2) \times 10^{-14}$
	1200	$7.0\ (1.3) \times 10^{-14}$	$-6.0\ (2.1) \times 10^{-14}$
	Q (kJ/mol) and D_0 (m^2/s)	—	—

Magnitudes are reported for either side of the B2/FCC interface in the diffusion couple. Note that only positive values were considered for the measurement of the activation energy and pre-exponential factor.

Table III. Comparison of Average Effective Interdiffusion Coefficients for Fe, Cr, and Ni in Fe-Cr-Ni and Al-Co-Cr-Fe-Ni Alloys at 1100 °C

	$Cr_{32.1}Fe_{15.8}Ni_{52.1}$ *vs* $Cr_0Fe_{52}Ni_{48}$		$Al_{48}Ni_{52}$ *vs* $Co_{25}Cr_{25}Fe_{25}Ni_{25}$
	$Cr_{32.1}Fe_{15.8}Ni_{52.1}$ to $Cr_{16.1}Fe_{33.5}Ni_{50.4}$	$Cr_{16.1}Fe_{33.5}Ni_{50.4}$ to $Cr_0Fe_{52}Ni_{48}$	$Al_{8.6}Co_{17.2}Cr_{25.6}Fe_{20.2}Ni_{28.3}$ to $Al_0Co_{25}Cr_{25}Fe_{25}Ni_{25}$
Component *i*	$\overline{\tilde{D}}_{i,L}^{\text{eff}}$ (m^2/s)	$\overline{\tilde{D}}_{i,R}^{\text{eff}}$ (m^2/s)	$\overline{\tilde{D}}_i^{\text{eff}}$ (m^2/s)
Cr	6.5×10^{-15}	6.2×10^{-15}	-2.7×10^{-14}
Fe	5.4×10^{-15}	5.5×10^{-15}	1.1×10^{-14}
Co	—	—	1.5×10^{-14}
Ni	2.2×10^{-16} (uphill diffusion)	1.7×10^{-15}	-1.2×10^{-14}
Al	—	—	2.1×10^{-14}

Table IV. Comparison of Average Effective Interdiffusion Coefficients for Individual Components at 1000 °C in Diffusion Couples, $Co_{20}Cr_{30}Fe_{20}Ni_{30}$ *vs* $Co_{30}Cr_{20}Fe_{30}Ni_{20}$, $Co_{10}Cr_{20}Fe_{15}Mn_{25}Ni_{30}$ *vs* $Co_{30}Cr_{20}Fe_{25}Mn_{15}Ni_{10}$, and $Al_{48}Ni_{52}$ *vs* $Co_{25}Cr_{25}Fe_{25}Ni_{25}$

Diffusion Couple	$Co_{20}Cr_{30}Fe_{20}Ni_{30}$ *vs* $Co_{30}Cr_{20}Fe_{30}Ni_{20}$	
Composition Range	$Co_{30}Cr_{20}Fe_{30}Ni_{20}$ to $Co_{25}Cr_{25}Fe_{25}Ni_{25}$	$Co_{25}Cr_{25}Fe_{25}Ni_{25}$ to $Co_{30}Cr_{20}Fe_{30}Ni_{20}$
$\bar{\tilde{D}}^{eff}_{Co}$ (m^2/s)	1.3×10^{-16}	1.8×10^{-16}
$\bar{\tilde{D}}^{eff}_{Cr}$ (m^2/s)	3.7×10^{-16}	4.5×10^{-16}
$\bar{\tilde{D}}^{eff}_{Fe}$ (m^2/s)	3.4×10^{-16}	3.0×10^{-16}
$\bar{\tilde{D}}^{eff}_{Ni}$ (m^2/s)	0.9×10^{-16}	0.5×10^{-16}
Diffusion couple	$Co_{10}Cr_{20}Fe_{15}Mn_{25}Ni_{30}$ *vs* $Co_{30}Cr_{20}Fe_{25}Mn_{15}Ni_{10}$	
Composition range	$Co_{10}Cr_{20}Fe_{15}Mn_{25}Ni_{30}$ to $Co_{20.1}Cr_{21.6}Fe_{19.6}Mn_{20.7}Ni_{18.4}$	$Co_{20.1}Cr_{21.6}Fe_{19.6}Mn_{20.7}Ni_{18.4}$ to $Co_{30}Cr_{20}Fe_{25}Mn_{15}Ni_{10}$
$\bar{\tilde{D}}^{eff}_{Co}$ (m^2/s)	2.5×10^{-16}	2.4×10^{-16}
$\bar{\tilde{D}}^{eff}_{Cr}$ (m^2/s)	-4.8×10^{-16} (uphill diffusion)	1.6×10^{-15}
$\bar{\tilde{D}}^{eff}_{Fe}$ (m^2/s)	4.8×10^{-16}	3.7×10^{-16}
$\bar{\tilde{D}}^{eff}_{Mn}$($m^2/s$)	2.7×10^{-16}	2.9×10^{-16}
$\bar{\tilde{D}}^{eff}_{Ni}$ (m^2/s)	1.9×10^{-16}	1.9×10^{-16}
Diffusion couple	$Al_{48}Ni_{52}$ *vs* $Co_{25}Cr_{25}Fe_{25}Ni_{25}$	
Composition range	$Al_{5.5}Co_{20.9}Cr_{25.4}Fe_{23.9}Ni_{24.3}$ to $Al_0Co_{25}Cr_{25}Fe_{25}Ni_{25}$	
$\bar{\tilde{D}}^{eff}_{Co}$ (m^2/s)	9.1×10^{-16}	
$\bar{\tilde{D}}^{eff}_{Cr}$($m^2/s$)	4.0×10^{-16}	
$\bar{\tilde{D}}^{eff}_{Fe}$ (m^2/s)	1.4×10^{-15}	
$\bar{\tilde{D}}^{eff}_{Ni}$ (m^2/s)	-2.2×10^{-15} (uphill diffusion)	
$\bar{\tilde{D}}^{eff}_{Al}$ (m^2/s)	9.3×10^{-16}	

CoCrFeNi and quinary CoCrFeNiMn systems. Diffusion of Co is the fastest in the Al-Co-Cr-Fe-Ni system. The Ni exhibited slower diffusion in the quaternary Co-Cr-Fe-Ni system than in the quinary Co-Cr-Fe-Ni-Mn and Al-Co-Cr-Fe-Ni systems. Therefore, a particular element in the lower order system does not necessarily have a larger interdiffusion coefficient than that in the higher order system.

It was initially proposed that higher order HEAs exhibit larger fluctuation in LPE due to variation in bond strength and atomic size mismatch.[8] The sluggish diffusion hypothesis (*i.e.*, core effect) originates from this large variation in LPE of atomic sites, which leads to the formation of temporary atomic traps on lattice sites (*i.e.*, highly stable low-energy sites) and, consequently, results in anomalously slow diffusion.[2,8] To that end, using the PEFs model,[27,28] described by Eq. [8], normalized PEFs; *i.e.*, p was determined for FeCrNi, CoCrFeNi, CoCrFeNiMn, and $Al_{0.45}$CoCrFeNi (at maximum solubility of Al in as-cast AlCoCrFeNi) alloys. Figure 3 compares the normalized PEFs as a function of temperature in ternary FeCrNi, quaternary CoCrFeNi, quinary CoCrFeNiMn, and $Al_{0.45}$CoCrFeNi alloys. Normalized PEFs are similar

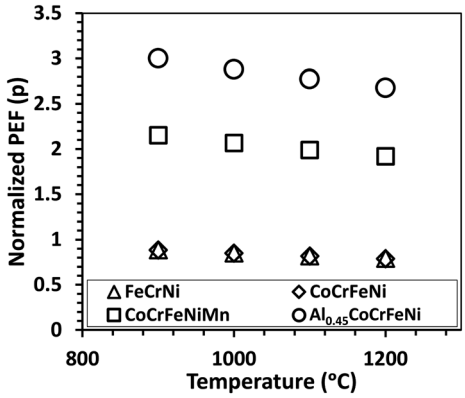

Fig. 3—Comparison of normalized PEFs in FeCrNi, CoCrFeNi, CoCrFeNiMn, and $Al_{0.45}$CoCrFeNi alloys.

for ternary and quaternary alloys but are approximately 2.5 times larger in quinary CoCrFeNiMn and 3.5 times larger in quinary $Al_{0.45}$CoCrFeNi. The magnitude of normalized PEFs provides an approximation on whether an atomic site will be an atomic trap or not; however, it does *not* give any information on the number

of trapping sites. On the one hand, with normalized PEFs ($p = \Delta E/k_BT$) < 1, the thermal energy fluctuations (k_BT) overcome the PEFs and atoms can easily escape the potential energy traps just by thermal vibrations. In this case, diffusion ideally should be enhanced. On the other hand, when normalized PEFs > 1, PEFs outweigh the thermal vibrations and diffusion should become sluggish. However, experimental observations did not quite align with the mathematical model, since diffusion kinetics were not necessarily sluggish for all elements in quinary alloys when compared with quaternary or ternary alloys. Even in two quinary systems, where normalized PEFs in $Al_{0.45}CoCrFeNi$ are 1.4 times larger than those in CoCrFeNiMn, diffusion coefficients were not lower for any elements in $Al_{0.45}CoCrFeNi$ alloy. This implies that the number of low-energy sites, *i.e.*, atomic traps, may not be sufficient during interdiffusion and trapping selected atoms may not necessarily result in a significant lowering of the interdiffusion coefficients.

V. SOLUBILITY LIMIT OF Al IN Al-Co-Cr-Fe-Ni ALLOY

The microstructure of Al-Co-Cr-Fe-Ni alloy depends on the concentration of Al. For instance, in as-cast $Al_xCoCrFeNi$ alloy, the FCC phase is stable when $x < 0.45$ (~ 10.1 at. pct Al), the BCC phase is stable when $x > 0.88$ (~ 18 at. pct Al), and the duplex (*i.e.*, FCC + BCC) phases are stable when $0.45 \le x \le 0.88$.[3,38] Therefore, the solubility limit of Al in nonequiatomic $Al_pCo_qCr_rFe_sNi_t$ alloy was also determined, in addition to interdiffusion coefficients, using the same diffusion couples. During interdiffusion of Al and Ni in $Co_{25}Cr_{25}Fe_{25}Ni_{25}$ (FCC) alloy, continuous nonequiatomic compositions of FCC $Al_pCo_qCr_rFe_sNi_t$ evolved; however, BCC or duplex phases were not observed in the starting microstructure of $Co_{25}Cr_{25}Fe_{25}Ni_{25}$ alloy. This observation suggests that the diffusion was significantly faster in FCC phase than in BCC phase.

Table V reports the maximum solubility limit of Al, measured using diffusion couples shown in Figure 2 in $Al_pCo_qCr_rFe_sNi_t$ alloys. The temperature-dependent solubility limit of Al in $Al_xCoCrFeNi$ alloy was examined using the pseudo-binary phase diagram between Al and equiatomic CoCrFeNi alloy, as shown in Figure 4(a).[39] Figure 4(b) compares the experimentally determined solubility limit of Al in nonequiatomic FCC $Al_pCo_qCr_rFe_sNi_t$ alloy, *via* diffusion couples, with the solubility limit of Al in equiatomic FCC $Al_xCoCrFeNi$ alloy determined from phase diagram. The maximum solubility of Al in as-cast $Al_xCoCrFeNi$ (*i.e.*, $x = 0.45$) alloy, as presented in Figure 4(b), demonstrates that from diffusion couples in $Al_pCo_qCr_rFe_sNi_t$ at 1100 °C and 1200 °C is higher than the solubility limit of Al in $Al_xCoCrFeNi$ alloy determined using phase diagram.

Figure 5(a) presents the configurational entropy of mixing at compositions corresponding to the maximum solubility limit of Al in $Al_pCo_qCr_rFe_sNi_t$ alloy, maximum solubility limit of Al in $Al_xCoCrFeNi$ alloy, and maximum solubility of Al in as-cast $Al_xCoCrFeNi$ (*i.e.*, $x = 0.45$) alloy. The experimentally determined

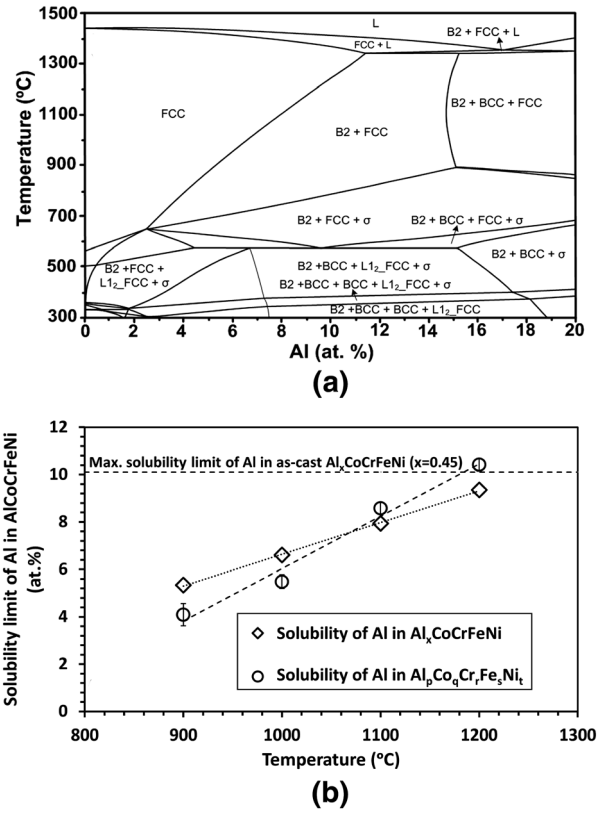

Fig. 4—(*a*) Pseudo-binary phase diagram between Al and equiatomic CoCrFeNi Ref. [39] (*b*) Comparison of the maximum solubility limit of Al as a function of temperature in $Al_pCo_qCr_rFe_sNi_t$ (from diffusion couple) and $Al_xCoCrFeNi$ (from phase diagram) HEAs.

Table V. Compositions of $Al_pCo_qCr_rFe_sNi_t$ Alloys Corresponding to the Maximum Solubility Limit of Al

Alloy System	T (°C)	Composition in Atomic Percent Corresponding to Maximum Solubility Limit of Al (Standard Deviation)				
		Al	Cr	Fe	Co	Ni
$Al_pCo_qCr_rFe_sNi_t$	900	4.08 (0.46)	25.83 (0.16)	24.86 (0.24)	22.25 (0.08)	22.98 (0.32)
	1000	5.48 (0.29)	25.44 (0.21)	23.86 (0.19)	20.91 (0.10)	24.30 (0.23)
	1100	8.57 (0.25)	25.19 (0.13)	20.72 (0.23)	17.65 (0.12)	27.85 (0.17)
	1200	10.42 (0.27)	23.15 (0.37)	20.01 (0.14)	15.99 (0.15)	30.44 (0.15)

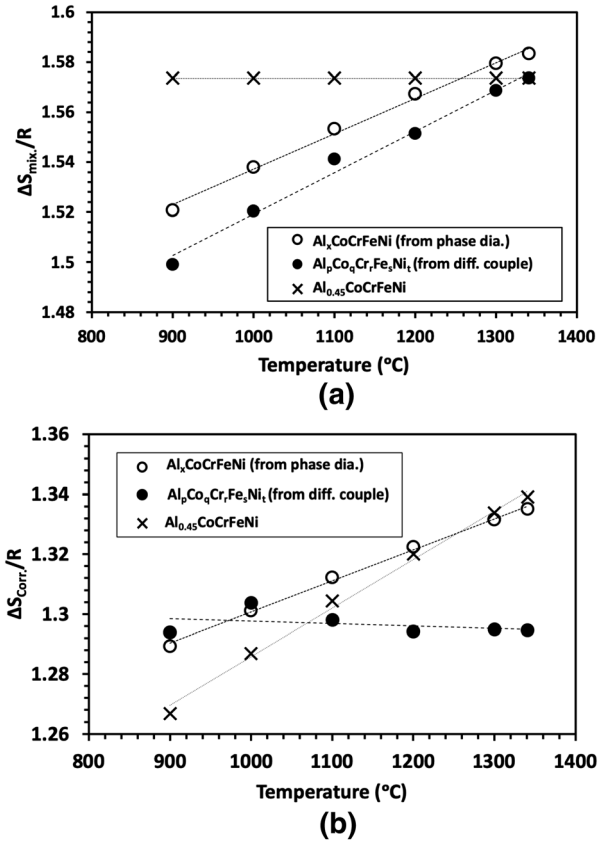

Fig. 5—Comparison of (*a*) entropy of mixing ($\Delta S_{mix}/R$) and (*b*) correlated entropy of mixing ($\Delta S_{corr}/R$) in $Al_pCo_qCr_rFe_sNi_t$ (using diffusion couple) and $Al_xCoCrFeNi$ (using phase diagram) for the compositions corresponding to the maximum solubility limits of Al and $Al_{0.45}CoCrFeNi$.

configurational entropy for $Al_pCo_qCr_rFe_sNi_t$ compositions between 900 °C and 1200 °C has been linearly extrapolated to a temperature (~ 1340.9 °C) corresponding to the maximum solubility limit of Al in $Al_xCoCrFeNi$, per the phase diagram. For all temperatures, the magnitude of configurational entropy in nonequiatomic $Al_pCo_qCr_rFe_sNi_t$ alloy is lower than that in equiatomic $Al_xCoCrFeNi$ alloy. Therefore, the entropy contribution ($-T\Delta S_{mix}$) in minimizing the overall free energy for stabilizing the single phase is lower in nonequiatomic $Al_pCo_qCr_rFe_sNi_t$ alloy than in equiatomic $Al_xCoCrFeNi$ alloy. He *et al.*[27] argued that the configurational entropy of mixing does not remain constant for a given composition as a function of temperature, due to the excess entropy term arising from the correlation effects between constituents elements, as described in Section III–B. Figure 5(b) presents the correlated configurational entropy as a function of temperature for the compositions corresponding to the maximum solubility limit of Al in $Al_pCo_qCr_rFe_sNi_t$, the maximum solubility limit of Al in $Al_xCoCrFeNi$, and the maximum solubility of Al in as-cast $Al_xCoCrFeNi$ (*i.e.*, $x = 0.45$) alloys. At 1100 °C and above, the magnitude of the correlated entropy of mixing is larger in equiatomic $Al_xCoCrFeNi$ alloy than in nonequiatomic $Al_pCo_qCr_rFe_sNi_t$ alloy. Therefore, the correlated entropy contribution ($-T\Delta S_{corr}$) in minimizing the overall free energy for stabilizing the single phase is greater in equiatomic $Al_pCo_qCr_rFe_sNi_t$ alloy than in nonequiatomic $Al_xCoCrFeNi$ alloy at 1100 °C and above.

Figure 6(a) presents the thermodynamic stability parameters based on mixing entropy, *i.e.*, ΔH_{mix}, $-T\Delta S_{mix}$, and ΔG_{mix}, and Figure 6(b) presents the thermodynamic stability parameters based on correlated configurational entropy, *i.e.*, ΔH_{mix}, $-T\Delta S_{corr}$, and ΔG_{corr}, as a function of temperature for equiatomic $Al_xCoCrFeNi$, nonequiatomic $Al_pCo_qCr_rFe_sNi_t$, and $Al_{0.45}CoCrFeNi$ alloys. Figure 6 demonstrates that for a given composition entropic contribution, ($-T\Delta S$) is significantly larger in magnitude than the enthalpy contribution (ΔH_{mix}) toward the overall thermodynamic stability of Al-Co-Cr-Fe-Ni alloy; *i.e.*, $|-T\Delta S| > |\Delta H|$ for all temperatures. This is in agreement with the general high entropy effect for HEAs. However, the magnitude of enthalpy (ΔH_{mix}) is not negligible in comparison to the entropy of mixing, *i.e.*, $|-T\Delta S_{mix}| / |\Delta H_{mix}| \approx 2.5$ to 3.5, or correlated entropy of mixing, *i.e.*, $|-T\Delta S_{corr}| / |\Delta H_{mix}| \approx 1.5$ to 2.5. Therefore, the role of enthalpy of mixing may become important with variation in the composition of the alloys, *i.e.*, variation in configurational entropies. Otto *et al.*[7] also suggested that configurational entropy alone may not always be a useful predictor of the formation of thermodynamically stable single-phase solid solutions. Figure 6 also suggests that the free energy of mixing (ΔG_{mix}) in $Al_pCo_qCr_rFe_sNi_t$ alloy is smaller than that in $Al_xCoCrFeNi$ at 1100 °C and above. The higher thermodynamic stability of $Al_pCo_qCr_rFe_sNi_t$ alloy at 1100 °C and above may be the possible reason for higher solubility of Al in nonequiatomic $Al_pCo_qCr_rFe_sNi_t$ alloy. The enthalpy of mixing (ΔH_{mix}) plays a significant role in minimizing the overall free energy of nonequiatomic $Al_pCo_qCr_rFe_sNi_t$, in comparison to equiatomic $Al_xCoCrFeNi$ at 1100 °C and above. This estimate can be drawn since the entropy contribution ($-T\Delta S$) is always lower in nonequiatomic $Al_pCo_qCr_rFe_sNi_t$ than in equiatomic $Al_xCoCrFeNi$ at 1100 °C and above. Figure 6 shows that ΔH_{mix} is lower for $Al_pCo_qCr_rFe_sNi_t$ at 1100 °C and above. Therefore, for a given composition of Al-Co-Cr-Fe-Ni HEAs, configurational entropy of mixing has a higher contribution in magnitude than enthalpy of mixing toward the overall thermodynamic stability; however, the nonequiatomic (*i.e.*, lower ΔS_{mix}) compositions may exhibit a similar or even higher thermodynamic stability due to higher enthalpy of mixing than the equiatomic (*i.e.*, highest ΔS_{mix}) counterparts at high temperature. It is also noteworthy that the role of enthalpy of mixing (ΔH_{mix}) cannot always be neglected when considering the stability of single-phase alloys with similar constituent elements but different compositions, *i.e.*, nonequiatomic $Al_pCo_qCr_rFe_sNi_t$ alloy *vs* equiatomic $Al_xCoCrFeNi$ alloy. It should be noted that the thermodynamic parameters of as-cast $Al_{0.45}CoCrFeNi$ alloy in Figures 5 and 6 have been presented to demonstrate the relative comparison to the $Al_pCo_qCr_rFe_sNi_t$ and $Al_xCoCrFeNi$ alloys. Ideally, under equilibrium, the maximum solubility of Al in FCC $Al_xCoCrFeNi$ alloy

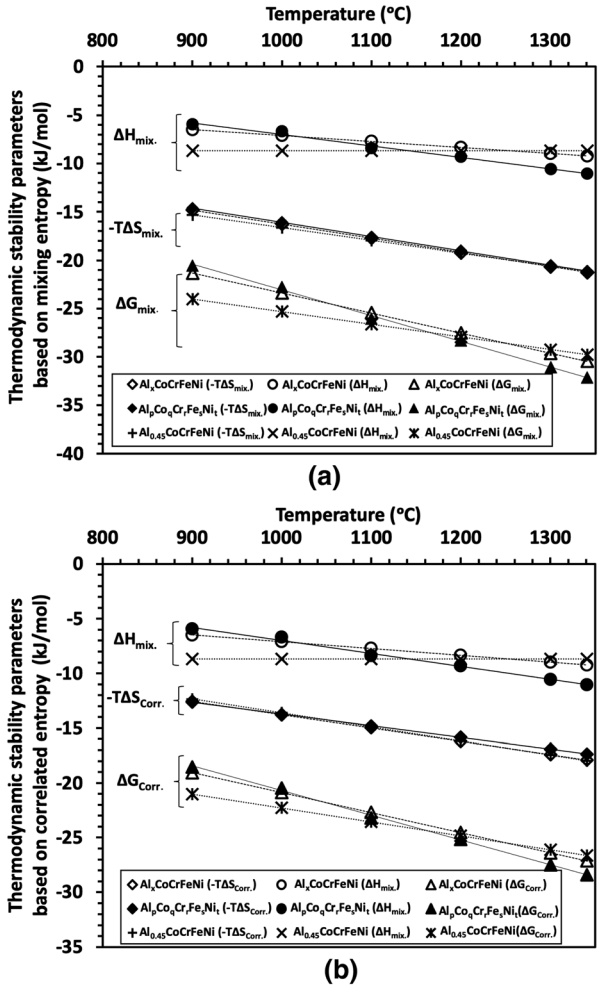

Fig. 6—(*a*) Comparison of thermodynamic stability parameters (ΔS, ΔH_{mix}, and ΔG) measured in the $Al_xCo_pCr_qFe_rNi_s$, $Al_xCoCrFeNi$, and $Al_{0.45}CoCrFeNi$ HEAs based on the (*a*) configurational entropy of mixing and (*b*) correlated entropy of mixing.

would decrease with a decrease in temperature below the melting point.

VI. PHASE FORMATION RULES

The high throughput combinatorial diffusion couple approach allows the determination of material characteristics/properties as a function of varying composition in a single experiment. To better understand the phase stability of various nonequiatomic $Al_pCo_qCr_rFe_sNi_t$ compositions generated in the diffusion couple, results were examined with respect to the existing empirical phase selection rules pertaining to multicomponent alloys, as described in Section III–C. The atomic size difference (δ) plays an important role for the formation of single-phase solid solution in HEAs. Therefore, all the solid solution phase formation predictors were examined against δ, as shown in Figure 7. Figure 7(a) shows the Ω *vs* δ plot for all the compositions developed in the diffusion couple. The Ω varies between 2 and 4.5, and δ varies between 0.6 and 4.5 pct. The smaller mismatch ($\delta \le 6.6$ pct) in atomic size[34,40] and $\Omega \ge 1.1$[34] has been suggested as a criterion for forming solid solution in HEAs. Figure 7(b) shows the ΔH_{mix} *vs* δ plot, where ΔH_{mix} for FCC Al-Co-Cr-Fe-Ni alloys was observed to vary from − 8.8 to − 3.8 kJ/mol. Guo *et al.*[40] reported that ΔH_{mix} for single-phase HEAs varied between − 11.6 and 3.2 kJ/mol and the corresponding δ values were small (< 6.6 pct). VEC also plays an important role in determining the structure of HEAs. Smaller values of VEC favor the formation of BCC phases, while higher VEC values favor the formation of FCC phases.[36] Figure 7(c) shows that VEC determined in this study for $Al_pCo_qCr_rFe_sNi_t$ alloys within diffusion couples varied between 7.8 and 8.25, which is in compliance with the VEC values (VEC > 7.5) suggested by Poletti and Battezzatti.[41] In general, $\Delta\chi$ is not considered to have strong influence on the phase stability in HEAs. Smaller $\Delta\chi$ (≤0.175) favors the formation of solid solution[42]; however, many exceptions to this rule were also reported.[43] In this study, $\Delta\chi$ varied between 0.097 and 0.116, as shown in Figure 7(d).

Phase formation rules described previously are generally accepted to predict the formation of single phase in HEAs. However, some exceptions have been documented in the literature pertaining to each predictor. For instance, the ΔH_{mix} *vs* δ plot has contradicting values in many studies,[34,40,44–46] which clearly demonstrates the inability of these rules to be applicable to all HEAs. In the present work, ΔH_{mix} varies between − 10 and − 4 kJ/mol, which is in compliance with the ΔH_{mix} values (*i.e.*, − 11.6 to 3.2 kJ/mol) suggested by Guo *et al.*[40]; however, Yang and Zhang[34] report a stable single phase up to − 17 kJ/mol. As mentioned previously, VEC in the present work varies between 7.8 and 8.25, in accordance with the VEC values for the formation of single phase suggested by Poletti and Battezzatti[41]; however, Guo *et al.*[36] strictly suggest VEC ≥ 8 for the stable single-phase formation in HEAs. Details of the single-phase prediction rules (and alloy design) and their capability (or limitations) have been discussed in detail by others.[47,48] The inability of generic phase prediction rules has motivated other researchers to introduce new variables based on geometric or thermodynamic factors to predict the phase formation (*i.e.*, single phase or intermetallics) in HEAs. The introduction of new parameters, such as the combination of the geometric-thermodynamic parameter Λ by Singh *et al.*,[49] thermodynamic parameter ϕ by Ye *et al.*[50] and King *et al.*,[51] and geometric parameter γ by Wang *et* al.,[52] demonstrates the inability of traditional phase formation rules to be applied to all HEAs. However, these new parameters also have some exceptions; therefore, there is no single standalone theory that could be applied universally to HEAs to predict the formation of single phase.

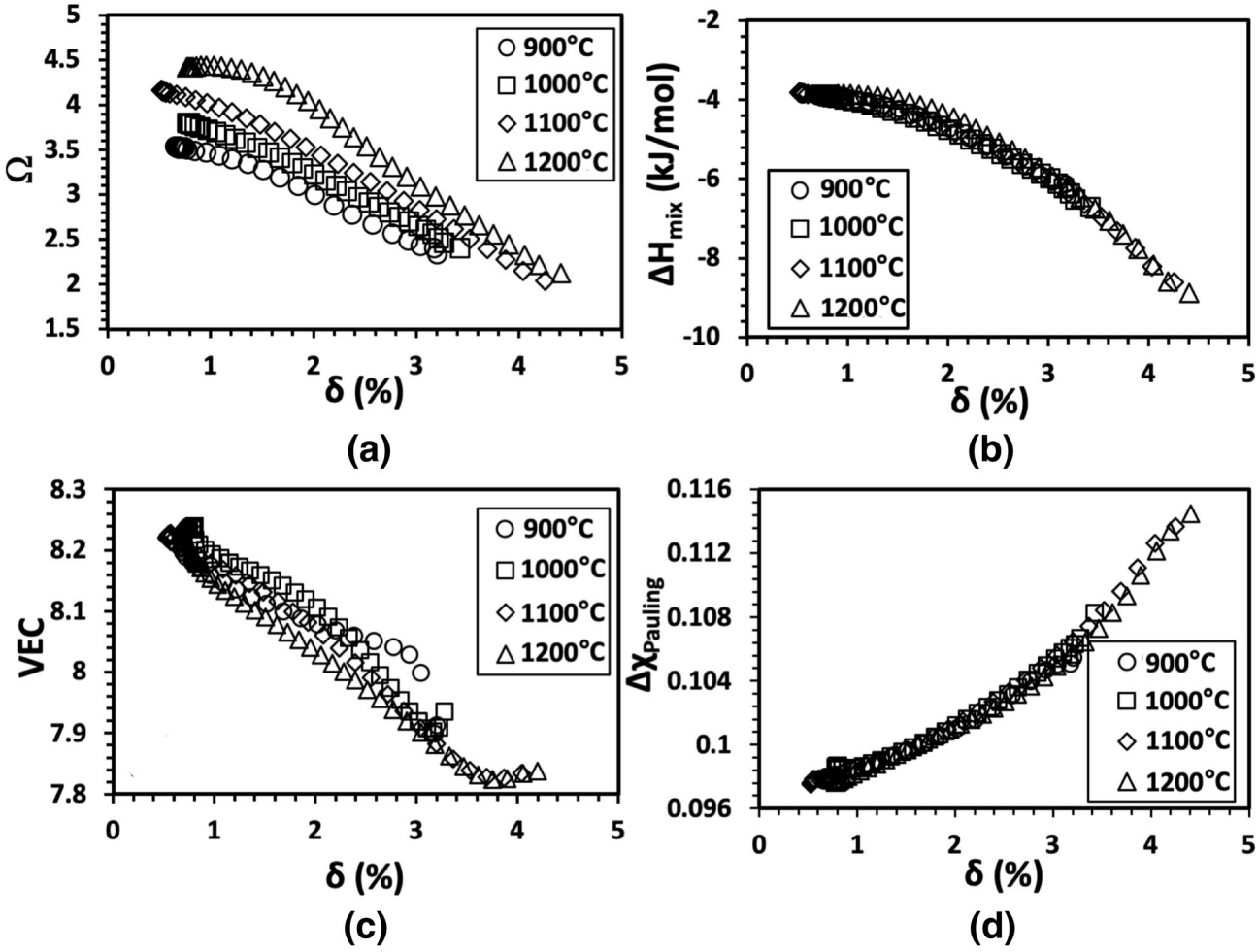

Fig. 7—Application of solid-solubility predictors to various nonequiatomic FCC $Al_pCo_qCr_rFe_sNi_t$ compositions generated in the diffusion couples: (*a*) Ω-δ, (*b*) ΔH_{mix}-δ, (*c*) VEC-δ, and (*d*) $\Delta\chi$-δ plots.

VII. CONCLUSIONS

The high throughput combinatorial diffusion couple approach was used to produce various nonequiatomic compositions of $Al_pCo_qCr_rFe_sNi_t$ HEAs by interdiffusing Al and Ni in equiatomic CoCrFeNi alloy. Interdiffusion coefficients of individual components in Al-Co-Cr-Fe-Ni alloy were determined, and a decrease in the interdiffusion coefficient was not observed for all components when compared to the interdiffusion coefficients in CoCrFeNi and FeCrNi systems. The maximum solubility limit of Al in nonequiatomic $Al_pCo_qCr_rFe_sNi_t$ was determined as a function of temperature and was compared with the solubility limit of Al in equiatomic $Al_xCoCrFeNi$ alloy. At temperatures of 1100 °C and above, nonequiatomic $Al_pCo_qCr_rFe_sNi_t$ alloy exhibited a higher solubility limit of Al, with higher thermodynamic stability than equiatomic $Al_xCoCrFeNi$ alloy. The enthalpy of mixing was determined to play an important role in the stabilization of single phase in the nonequiatomic $Al_pCo_qCr_rFe_sNi_t$ alloy than in the equiatomic $Al_xCoCrFeNi$ alloy. In general, entropy makes a significant contribution toward the overall thermodynamic stability of a given HEA composition; however, the role of enthalpy of mixing cannot be neglected when comparing the thermodynamic stabilities of different compositions (*e.g.*, equiatomic $Al_xCoCrFeNi$ *vs* nonequiatomic $Al_pCo_qCr_rFe_sNi_t$). Therefore, equiatomic compositions, which correspond to the highest mixing entropy, may not always yield the lowest free energy (*i.e.*, thermodynamic stability) at high temperature. All compositions in nonequiatomic $Al_xCo_pCr_qFe_rNi_s$ alloys produced within diffusion couples were observed to follow the generally accepted existing empirical rules for the formation of single phase in HEAs.

REFERENCES

1. J.W. Yeh: *Ann. Chim. Sci. Mater.*, 2006, vol. 31, pp. 633–48.
2. E. Pickering and N. Jones: *Int. Mater. Rev.*, 2016, vol. 61, pp. 183–202.
3. W.R. Wang, W.L. Wang, S.C. Wang, Y.C. Tsai, C.H. Lai, and J.W. Yeh: *Intermetallics*, 2012, vol. 26, pp. 44–51.
4. J. He, W. Liu, H. Wang, Y. Wu, X. Liu, T. Nieh, and Z. Lu: *Acta Mater.*, 2014, vol. 62, pp. 105–13.

5. Y. Guo, L. Liu, Y. Zhang, J. Qi, B. Wang, Z. Zhao, J. Shang, and J. Xiang: *J. Mater. Res.*, 2018, vol. 33, pp. 3258–65.
6. F. Zhang, C. Zhang, S.-L. Chen, J. Zhu, W.-S. Cao, and U.R. Kattner: *CALPHAD*, 2014, vol. 45, pp. 1–10.
7. F. Otto, Y. Yang, H. Bei, and E.P. George: *Acta Mater.*, 2013, vol. 61, pp. 2628–38.
8. K.Y. Tsai, M.H. Tsai, and J.W. Yeh: *Acta Mater.*, 2013, vol. 61, pp. 4887–97.
9. M. Vaidya, S. Trubel, B. Murty, G. Wilde, and S.V. Divinski: *J. Alloys Compd.*, 2016, vol. 688, pp. 994–1001.
10. M. Vaidya, K. Pradeep, B. Murty, G. Wilde, and S. Divinski: *Acta Mater.*, 2018, vol. 146, pp. 211–24.
11. M. Vaidya, K. Pradeep, B. Murty, G. Wilde, and S. Divinski: *Sci. Rep.*, 2017, vol. 7, pp. 1–11.
12. J. Dąbrowa, W. Kucza, G. Cieślak, T. Kulik, M. Danielewski, and J.-W. Yeh: *J. Alloys Compd.*, 2016, vol. 674, pp. 455–62.
13. D. Beke and G. Erdélyi: *Mater. Lett.*, 2016, vol. 164, pp. 111–13.
14. T.R. Paul, I.V. Belova, and G.E. Murch: *Mater. Chem. Phys.*, 2018, vol. 210, pp. 301–08.
15. A. Allnatt, T. Paul, I. Belova, and G. Murch: *Philos. Mag.*, 2016, vol. 96, pp. 2969–85.
16. K. Kulkarni and G.P.S. Chauhan: *AIP Adv.*, 2015, vol. 5, pp. 1–7.
17. V. Verma, A. Tripathi, and K.N. Kulkarni: *J. Phase Equilb. Diffus.*, 2017, vol. 38, pp. 445–56.
18. A. Mehta, L. Zhou, E.A. Schulz, D.D. Keiser, J.I. Cole, and Y. Sohn: *J. Phase Equilb. Diffus.*, 2018, vol. 39, pp. 246–54.
19. Y. Park, R. Newell, A. Mehta, D. Keiser, Jr, and Y. Sohn: *J. Nucl. Mater.*, 2018, vol. 502, pp. 42–50.
20. E.A. Schulz, A. Mehta, I.V. Belova, G.E. Murch, and Y. Sohn: *J. Phase Equilb. Diffus.*, 2018, vol. 39, pp. 862–69.
21. L. Onsager: *Ann. N. Y. Acad. Sci.*, 1945, vol. 46, pp. 241–65.
22. M. Dayananda and C. Kim: *Metall. Mater. Trans. A*, 1979, vol. 10A, pp. 1333–39.
23. J.S. Kirkaldy: *Can. J. Phys.*, 1957, vol. 35, pp. 435–40.
24. M. Dayananda and Y. Sohn: *Scripta Mater.*, 1996, vol. 35, pp. 683–88.
25. D. Liu, L. Zhang, Y. Du, H. Xu, and Z. Jin: *J. Alloys Compd.*, 2013, vol. 566, pp. 156–63.
26. K. Cheng, D. Liu, L. Zhang, Y. Du, S. Liu, and C. Tang: *J. Alloys Compd.*, 2013, vol. 579, pp. 124–31.
27. Q. He, Y. Ye, and Y. Yang: *J. Appl. Phys.*, 2016, vol. 120, pp. 1–10.
28. Q. He, Y. Ye, and Y. Yang: *J. Phase Equilb. Diffus.*, 2017, vol. 38, pp. 416–25.
29. H. Bakker: *Enthalpies in Alloys: Miedema's Semi-Empirical Model*, Enfield Publishing & Distribution Company, Enfield, NH, 1998.
30. A. Takeuchi and A. Inoue: *Mater. Trans.*, 2005, vol. 46, pp. 2817–29.
31. I. Ford: *Statistical Physics: An Entropic Approach*, 1st ed., Wiley, Hoboken, NJ, 2013.
32. S. Fang, X. Xiao, L. Xia, W. Li, and Y. Dong: *J. Non-Cryst. Solids*, 2013, vol. 321, pp. 120–25.
33. A. Takeuchi, A. Inoue, and Y. Dong: *Mater. Trans., JIM*, 2000, vol. 41, pp. 1372–78.
34. X. Yang and Y. Zhang: *Mater. Chem. Phys.*, 2012, vol. 132, pp. 233–38.
35. U. Mizutani: *Hume-Rothery Rules for Structurally Complex Alloy Phases*, CRC Press, Boca Raton, FL, 2016.
36. S. Guo, C. Ng, J. Lu, and C. Liu: *J. Appl. Phys.*, 2011, vol. 109, pp. 1–5.
37. J.G. Duh and M.A. Dayananda: *Diffus. Def. Data*, 1985, vol. 39, pp. 1–50.
38. Y.F. Kao, T.J. Chen, S.K. Chen, and J.W. Yeh: *J. Alloys Compd.*, 2009, vol. 488, pp. 57–64.
39. M. Komarasamy, T. Wang, K. Liu, L. Reza-Nieto, and R.S. Mishra: *Scripta Mater.*, 2019, vol. 162, pp. 38–43.
40. S. Guo, Q. Hu, C. Ng, and C. Liu: *Intermetallics*, 2013, vol. 41, pp. 96–103.
41. M. Poletti and L. Battezzati: *Acta Mater.*, 2014, vol. 75, pp. 297–306.
42. X. Yang, S. Chen, J. Cotton, and Y. Zhang: *JOM*, 2014, vol. 66, pp. 2009–20.
43. Y. Dong, Y. Lu, L. Jiang, T. Wang, and T. Li: *Intermetallics*, 2014, vol. 52, pp. 105–09.
44. Y. Zhang, Y.J. Zhou, J.P. Lin, G.L. Chen, and P.K. Liaw: *Adv. Eng. Mater.*, 2008, vol. 10, pp. 534–38.
45. M.X. Ren, B.S. Li, and H.Z. Fu: *Trans. Nonferr. Met. Soc. China*, 2013, vol. 23, pp. 991–95.
46. A. Takeuchi, K. Amiya, T. Wada, K. Yubuta, W. Zhang, and A. Makino: *Entropy*, 2013, vol. 15, pp. 3810–21.
47. L. Jiang, Y. Lu, H. Jiang, T. Wang, B. Wei, Z. Cao, and T. Li: *Mater. Sci. Technol.*, 2016, vol. 32, pp. 588–92.
48. D. Miracle and O. Senkov: *Acta Mater.*, 2017, vol. 122, pp. 448–511.
49. A.K. Singh, N. Kumar, A. Dwivedi, and A. Subramaniam: *Intermetallics*, 2014, vol. 53, pp. 112–19.
50. Y. Ye, Q. Wang, J. Lu, C. Liu, and Y. Yang: *Scripta Mater.*, 2015, vol. 104, pp. 53–55.
51. D. King, S. Middleburgh, A. McGregor, and M. Cortie: *Acta Mater.*, 2016, vol. 104, pp. 172–79.
52. Z. Wang, Y. Huang, Y. Yang, J. Wang, and C. Liu: *Scripta Mater.*, 2015, vol. 94, pp. 28–31.